climate

MDPI

Article

Future Projections of Clouds and Precipitation Patterns in South Asia: Insights from CMIP6 Multi-Model Ensemble Under SSP5 Scenarios

Praneta Khardekar [1,2], Rohini Lakshman Bhawar [2,*], Vinay Kumar [3] and Hemantkumar S. Chaudhari [4]

[1] Department of Physics, Savitribai Phule Pune University, Pune 411007, India; khardekarpraneta@gmail.com
[2] Department of Atmospheric and Space Science, Savitribai Phule Pune University, Pune 411007, India
[3] Department of Atmospheric Science, Environmental Science and Physics, University of the Incarnate Word, San Antonio, TX 78209, USA; vkumar@uiwtx.edu
[4] Indian Institute of Tropical Meteorology (IITM), Pune 411008, India; hemantkumar@tropmet.res.in
* Correspondence: rbhawar@unipune.ac.in

Abstract: Projecting future changes in monsoon rainfall is crucial for effective water resource management, food security, and livestock sustainability in South Asia. This study assesses precipitation, total cloud cover (categorized by cloud top pressure), and outgoing longwave radiation (OLR) across the region using Coupled Model Intercomparison Project Phase 6 (CMIP6) data. A multi-model ensemble (MME) approach is employed to analyze future projections under the Shared Socio-Economic Pathway (SSP5-8.5) scenario, which assumes radiative forcing will reach 8.5 W/m^2 by 2100. The MME projects a ~1.5 mm/day increase in total rainfall during 2081–2100. Convective and stratiform precipitation are expected to expand spatially, with convective rainfall increasing from 3 mm/day in historical simulations to 3.302 mm/day in the far future. Stratiform precipitation also shows an increase from 0.822 mm/day to 0.962 mm/day over the same period. A notable decrease in OLR (~60 W/m^2 along the Western Ghats) and an increase in high cloud cover suggest intensified monsoon rainfall. The pattern correlation coefficient (PCC) reveals reduced OLR in future scenarios (PCC ~0.77 vs. ~0.81 historically), likely due to cloud feedback mechanisms. These results highlight enhanced monsoonal activity under warming scenarios, with implications for regional climate adaptation.

Keywords: shared socio-economic pathways (SSP's); CMIP6; multi-model ensemble; high cloud cover

check for updates

Academic Editor: Konstantia Tolika

Received: 28 December 2024
Revised: 27 January 2025
Accepted: 4 February 2025
Published: 8 February 2025

Citation: Khardekar, P.; Bhawar, R.L.; Kumar, V.; Chaudhari, H.S. Future Projections of Clouds and Precipitation Patterns in South Asia: Insights from CMIP6 Multi-Model Ensemble Under SSP5 Scenarios. *Climate* **2025**, *13*, 36. https://doi.org/10.3390/cli13020036

Copyright: © 2025 by the authors. Licensee MDPI, Basel, Switzerland. This article is an open access article distributed under the terms and conditions of the Creative Commons Attribution (CC BY) license (https://creativecommons.org/licenses/by/4.0/).

1. Introduction

The water availability and food security of India depend heavily on the Indian summer monsoon rainfall, which affects the lives of a large population [1,2]. Nearly 80% of the annual precipitation over India occurs during the monsoon months from June to September [3], and the released latent heat plays a crucial role not only in atmospheric circulations but also in the radiative heat budget of the region [4]. Agriculture, being a predominant occupation, remains vital to the country's development, even though India has made significant progress in the service and industrial sectors. Extreme rainfall events and crop failures have adversely impacted millions of inhabitants and the national economy. Therefore, it is critical to understand how the monsoon will change due to future global warming and increased greenhouse gas emissions, in order to enable effective adaptation measures.

Observations indicate significant trends in rainfall across various regions of India. Some subdivisions show a positive trend in monsoon rainfall, others display a significant

negative trend, while certain small regions exhibit no significant trends [5,6]. In the same context, numerous studies have demonstrated that GPCP data are reliable and highly effective for evaluating precipitation [7]. Similarly, another study describes that overall, GPCP provides a more accurate representation of oceanic precipitation compared to CMAP. However, over land, both products are generally similar. Nonetheless, differences in their merging algorithms can occasionally result in significant discrepancies in sensitive regions [8]. However, the GPCP dataset is widely used. Past studies suggest an increase in mean Indian summer monsoon precipitation and inter-annual variability under enhanced warming scenarios [9–12]. A study [13], pointed out that, Intergovernmental Panel on Climate Change Fourth Assessment Report (IPCC AR4) models, projected an increase in monsoon precipitation strength. Similarly, ref. [14] revealed monsoon intensification due to increased moisture content under elevated CO_2 forcing. The IPCC Fifth Assessment Report (AR5) also indicates an expansion in global monsoon area, intensity, and precipitation by the end of the 21st century, along with shifts in onset dates. All-India precipitation under the baseline scenario is projected to increase by 4% to 5% by the 2030s and by 6% to 14% by the late 21st century (2080s) compared to the 1961–1990 simulations in RCP (Representative Concentration Pathway) and CMIP5 (Coupled Model Intercomparison Project Phase-5) MME scenarios [15–18]. A study by [19] identified MIROC5 as the most skillful model among CMIP5 GCMs and ACCESS-CM2 among CMIP6 GCMs. Overall, CMIP6 MME showed a significant improvement over CMIP5 MME in simulating rainfall over Bangladesh. Similarly, another study based on climate type analysis considered that NESM3, the most versatile model, ranks in the top 10 for 14 out of 29 global climate types, with a maximum CRI (Composite Rating Index) of only 0.7. Similarly, MPI-ESM-1-2-HAM achieves a CRI of 0.69 in Southern Europe, it only ranks in the top 10 in seven regions globally. The study also highlights that no single model performs well on a global scale [20]. The representation of precipitation in various models participating in CMIP6 also shows variations while depicting the annual cycle of mean rainfall along the Indian region [14]. Studies by [21] have shown that the superposed epoch analysis of PW (precipitable water) variation, relative to the arrival and withdrawal dates of the SWM (Southwest Monsoon), reveals that across various parts of the country, for example over Kolkata, precipitable water (mm) increases from 48.62 to 61.4 during monsoon arrival, while during withdrawal, it decreases from 48.62 to 22.55. Countries in the maritime continent experience the highest number of precipitation events with magnitudes exceeding 10 mm (R10) [22].

However, projecting the inter-annual variability of South Asian monsoon rainfall remains a significant challenge [23,24]. Factors such as tropical sea surface temperatures and extra-tropical oscillations like the Atlantic Multidecadal Oscillation further complicate projections [25].

Clouds play a critical role in maintaining the Earth's radiation budget by reflecting incoming solar radiation and absorbing outgoing longwave radiation [26]. Overall, variations in cloud water have the greatest impact on net cloud forcing, with high cloud variations primarily affecting long-wave cloud forcing and cloud water changes contributing most significantly to short-wave cloud forcing [27]. Climate sensitivity is generally higher in CMIP6 compared to CMIP5, primarily due to stronger positive low cloud feedback. This results from larger reductions in low cloud cover and smaller increases in low cloud water content, especially in the extra tropics [28]. Cloud-climate feedback significantly influences the equilibrium of climate sensitivity, affecting the magnitude and pace of future climate change [28,29]. Despite their importance, clouds remain challenging to accurately simulate in global climate models due to the complexity of relevant physics, which involves nonlinear processes across various temporal and spatial scales. The biases in climate models highlight the role of clouds in contributing to uncertainties in climate projections [29]. As

a result, simulating cloud processes requires extensive parameterization, including the formation, growth, and sedimentation of water particles [30,31].

Accurately evaluating clouds in global climate models is crucial for assessing model's skills in reproducing observed climate and projecting future changes. The Coupled Model Intercomparison Project (CMIP), a World Climate Research Programme (WCRP) initiative, provides coordinated simulations with Earth System Models (ESMs) for historical and future scenarios [32]. The newly developed Scenario Model Intercomparison Project (ScenarioMIP) within CMIP6 focuses on climate projections based on scenarios addressing societal concerns about climate change mitigation and adaptation. These projections are driven by new emissions and land-use scenarios with radiative forcing ranging from low to high-emission pathways [33,34].

CMIP6 models demonstrate improvements in large-scale climatological patterns of temperature, water vapor, and zonal wind speed compared to CMIP3 and CMIP5 although significant biases in cloud properties persist in specific regions [35,36]. Understanding errors in stratiform and convective cloud schemes remains a challenge, but accurate representation of these processes is essential for improving simulations of monsoon variability [37].

Past studies indicate that heavy precipitation events will intensify more than lighter events under a warming climate [38,39]. CMIP5 models show changes in cloud cover and type in response to anthropogenic forcing [40]. This study examines annual precipitation distribution, including convective and large-scale components, using CMIP6 models. Additionally, it investigates how total cloud fraction, and its levels will respond to increased radiative forcing (8.5 W/m^2) driven by greenhouse gas emissions over South Asia.

2. Materials and Methods

2.1. CMIP6 Models

In this study, we have utilized the Coupled Model Intercomparison Project Phase 6 (CMIP6) [32] individual model simulations for analysis. The models and their key references are listed in Table 1. All model data are freely available via the Earth System Grid Federation (ESGF). For the analysis presented here, the variables considered include total precipitation (PR), total cloud fraction (TCF), low-level cloud fraction (LCF), mid-level cloud fraction (MCF), high-level cloud fraction (HCF), and outgoing longwave radiation (OLR) for both future (2015–2100) and historical simulations (1850–2014).

Table 1. CMIP6 Models and their key references along with the resolution.

No.	CMIP6 Model Name	Country	Horizontal Resolution (In Degree)	Key References
1	E3SM-1-0	USA	0.90 × 0.90	[41]
2	IPSL-CM6A-LR	France	2.50 × 1.30	[42]
3	MIROC6	Japan	1.40 × 1.40	[43]
4	MRI-ESM2-0	Japan	1.10 × 1.10	[44]

Convective precipitation is directly available on the CMIP6 platform, while stratiform precipitation is derived from total and convective precipitation. The Shared Socioeconomic Pathway (SSP) 5–8.5 simulations (2015–2100) considered in this study assume an increase in greenhouse gas emissions due to high fossil fuel dependency and rapid economic growth [34]. We have considered r1i1p1f1 ensemble id for all models.

A multi-model ensemble of CMIP6 is generated from the available models for the present analysis. To ensure a fair comparison, all CMIP6 models have been re-gridded to a fixed latitude-longitude grid (1° × 1°).

2.2. Observational Datasets

Monthly data for total cloud fraction (TCF) were obtained from the GCM-Oriented CALIPSO Cloud Product (GOCCP, [45]) (GCM-Oriented Cloud-Aerosol Lidar and Infrared Pathfinder Satellite Observation (CALIPSO) Cloud Product) for the available period of 2006–2017 (12 years). This product is widely used to evaluate model cloudiness [46,47]. Monthly rainfall datasets were sourced from the Global Precipitation Climatology Project Version 2.3 (GPCP, [48]) covering the period from 1979 to the present. Climatology is considered in accordance with historical simulations (1984–2014).

Outgoing longwave radiation (OLR) data were obtained from the National Oceanic and Atmospheric Administration (NOAA), available from 1979 to 2022, with spatial coverage of 2.5° × 2.5° [49]. Similarly, observational datasets for convective and large-scale rainfall were sourced from the TRMM Precipitation Radar (PR) data for the period 1998–2010 [50]. All observational datasets were re-gridded to a 1° × 1° grid for consistency.

3. Results

3.1. Climatological Mean and Variability of Total Rainfall and Cloud Cover in Future Projections

To analyze the annual variability of the Indian Summer Monsoon, a temporal time series is presented in Figure 1 for both historical and future scenarios. The annual cycle over the Indian subcontinent (65° E–95° E, 5° N–40° N) highlights an increase in precipitation under global warming scenarios.

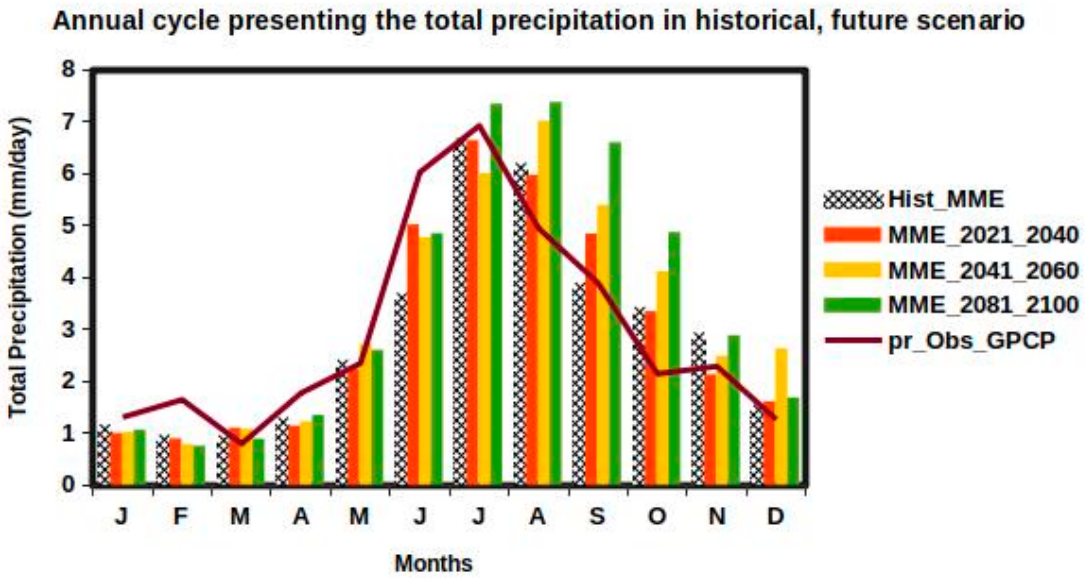


Figure 1. Annual cycle representing the total precipitation along the Indian region 65° E–95° E, 5° N–40° N) in the near-term (2021–2040), mid-term (2041–2060), far-future term (2081–2100), and historical (1984–2014) simulation compared with the observational dataset (GPCP).

The observational dataset provides the baseline for assessing precipitation trends. Historical simulations replicate past conditions and serve as a benchmark. Future projections show a progressive increase in October precipitation: approximately 1.5 mm/day higher in the far-future (2081–2100) compared to historical levels. The mid-term period (2041–2060) also shows increased precipitation relative to the near-term (2021–2040) and historical data, indicating a consistent upward trend over time due to climate change. A qualitative analysis of precipitation, including onset, duration, and withdrawal characteristics, is derived from the space–time rainfall patterns shown as a latitudinal variation in mean rainfall averaged over longitudes (40° E–110° E) (Figure 2). The Hovmöller plot effectively depicts the seasonal migration of rainfall across the Northern Hemisphere, with the Multi-Model

Ensemble (MME) providing an accurate representation. The Indian monsoon fully develops in June, gradually shifts northward, and withdraws rapidly in September. Figure 2 captures the northward seasonal migration of the ITCZ (Inter-tropical Convergence Zone) in response to seasonaatitude variation.

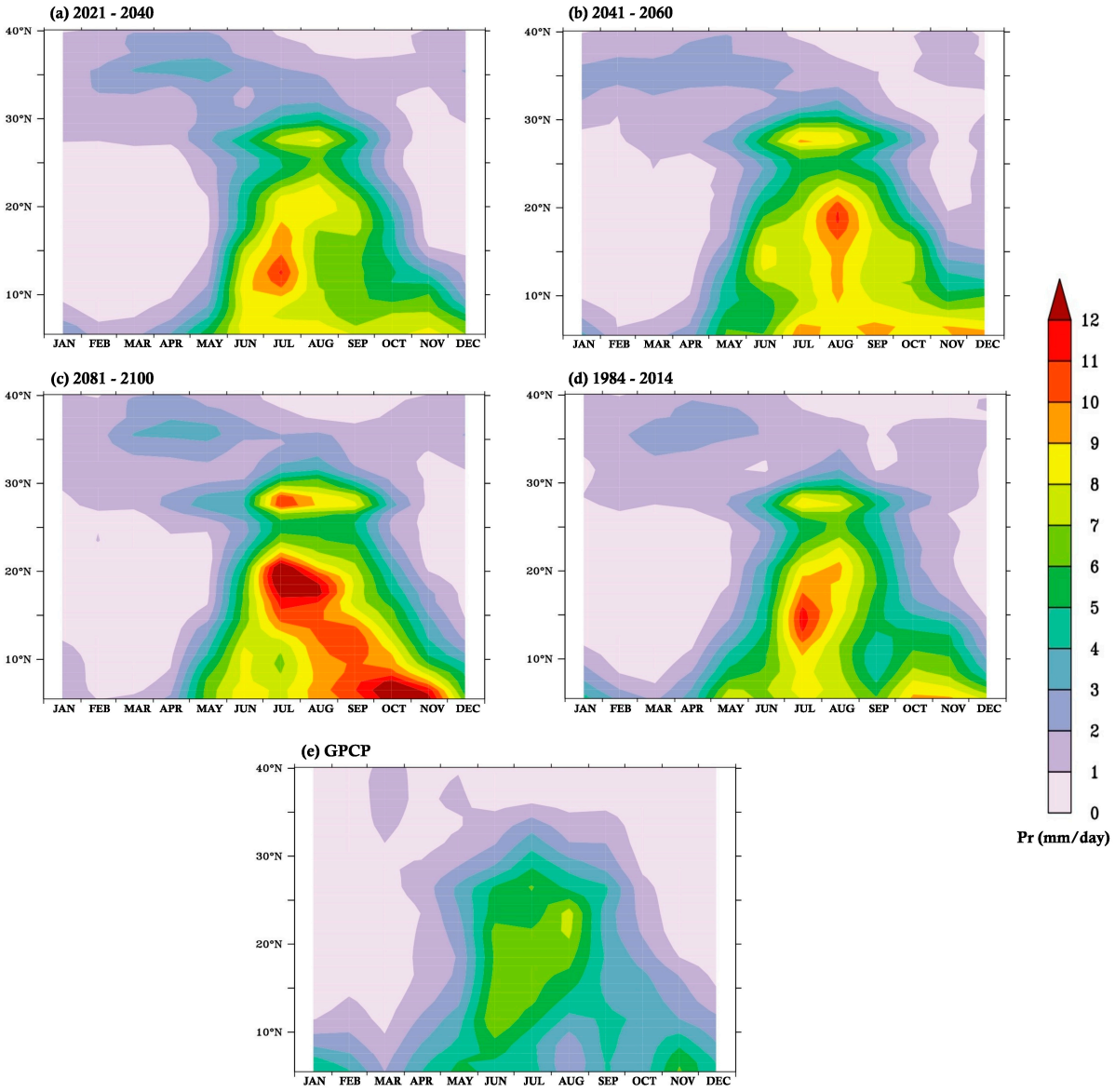


Figure 2. Time-latitude plot for precipitation (**a**) near- (2021–2040), (**b**) mid- (2041–2060), (**c**) far-future term (2081–2100), along with (**d**) historical (1984–2014) and (**e**) observational (GPCP) along the South Asian region (40° E–110° E; 20° S–40° N).

The observational dataset provides a baseline for rainfall patterns, showing maxima around 3 mm/day. An increase in precipitation levels can be seen during the mean monsoon period in historical simulations as compared to observational dataset with rainfall diminishing north of 5° N in September. In the near-term (2021–2040, Figure 2a), rainfall maxima (~2 mm/day) migrate up to 28° N. In the mid-term (2041–2060, Figure 2b), rainfall extends in September, unlike historical trends. The far-future period (2081–2100, Figure 2c) projects a significant increase in rainfall (~5 mm/day), surpassing observations and indicating intensification under future climate scenarios. A belt-like structure of extreme convective activity is identified, extending into the post-monsoon period in the Southern region, suggesting intensified rainfall patterns across South Asia in the future. Despite the

critical role of clouds in regulating rainfall variability [51] through heating control [52,53], Indian Summer Monsoon clouds remain underexplored in both past and future projections. To address this gap, an analysis of total cloud cover over the Indian region will be conducted temporally and spatially using observational data (CALIPSO-GOCCP) alongside historical simulations.

The temporal time series of total cloud fraction for the observational, historical, near, mid, and far-future periods under SSP5-8.5 is shown in Figure 3.

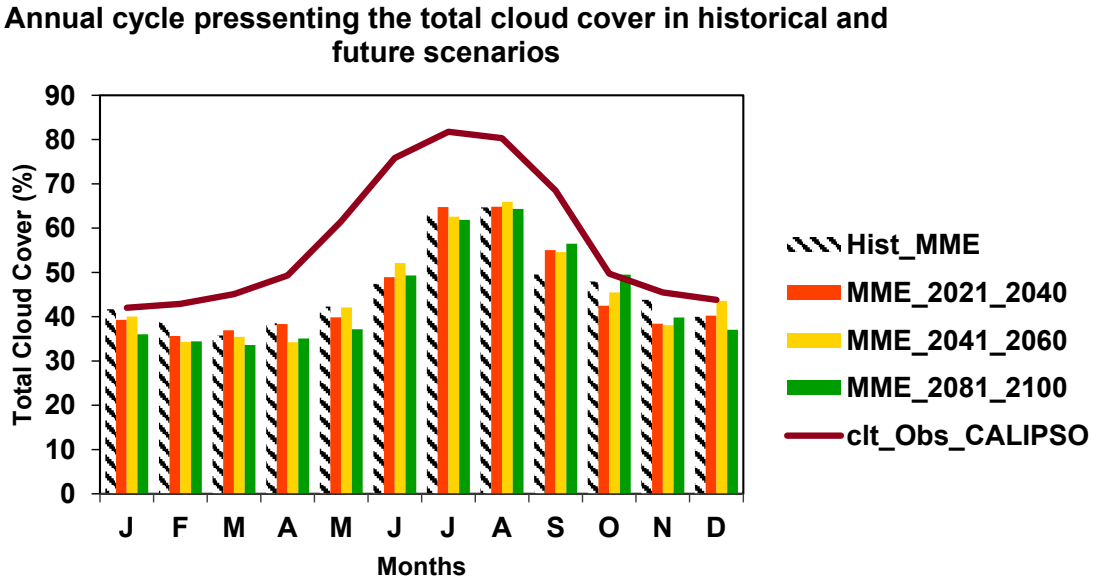


Figure 3. Annual representation of total cloud fraction along the Indian region (65° E–95° E, 5° N–40° N) in the near-term (2021–2040), mid-term (2041–2060), far-future (2081–2100), and historical compared with the observational dataset (CALIPSO-GOCCP).

The following statistical parameters are calculated in order to know the ability of the model to simulate hindcast simulation (Table 2). For this analysis, we have made three categories of precipitation: (i) less than 3 mm/day (considered as light rain), (ii) 3–5 mm/day (moderate precipitation), (iii) greater than 5 mm/day (heavy precipitation). This shows that the MRI model performs better for light rainfall (<3 mm/day), while the E3SM model excels for medium rainfall (3–5 mm/day) and outperforms others for heavy rainfall (>5 mm/day).

The observational dataset provides a reference for assessing cloud cover trends across the Indian region (65° E–95° E, 5° N–40° N) and South Asia (40° E–110° E, 20° S–40° N). Historical simulations align closely with observational data, effectively capturing total cloud cover levels across the annual cycle. Future projections show a deviation from historical simulations, with challenges in capturing total cloud cover levels accurately over the Indian region. However, spatial analysis across South Asia (Figure 4) reveals notable patterns. In the near-term (2021–2040), cloud cover increases by ~10% over the Equatorial Indian Ocean, Western Ghats, and Tibetan Plateau compared to historical simulations. Mid- and far-future projections continue to show enhanced cloud cover over oceanic regions relative to land areas. The mean total cloud cover rises across all future periods, with averages of 55.49% (near-term), 55.48% (mid-term), and 54.45% (far-future) compared to 53.87% in historical simulations. This indicates a trend of amplified cloud cover, particularly in oceanic regions, driven by projected climatic changes.

Table 2. Skill score of models for precipitation categorized in various bins.

Models	Probability of Detection (POD)	Probability of False Detection (POFD)	Heidke Skill Score (HSS)
	Less than 3 mm/day		
E3SM	0.915	0.183	0.729
MIROC6	0.917	0.329	0.588
IPSL	0.68	0.75	−0.071
MRI	1	0.57	0.419
	Between 3 and 5 mm/day		
E3SM	0.666	0.119	0.5552
MIROC6	0.576	0.097	0.4934
IPSL	0.23	0.29	−0.064
MRI	0.41	0.05	0.37
	Greater than 5 mm/day		
E3SM	0.444	0.163	0.302
MIROC6	0.222	0.031	0.215
IPSL	0	0.01	−0.01
MRI	0	0	0

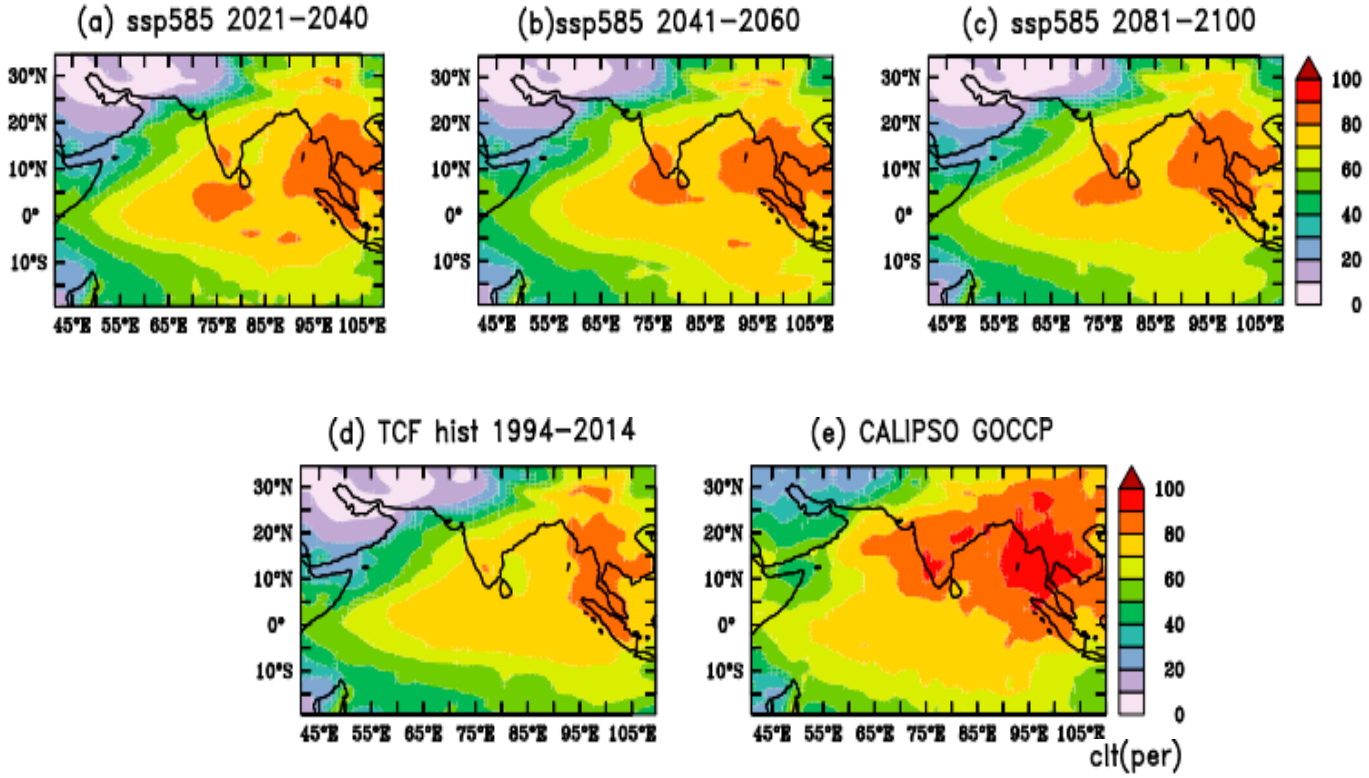


Figure 4. Spatial pattern of total cloud fraction (%) for JJAS of MME in near- (2021–2040), mid- (2041–2060), and far-future (2081–2100) terms in SSP5-8.5 scenario; compared with historical (1984–2014) and observational dataset (CALIPSO-GOCCP) along the South Asian region.

3.2. Convective and Large-Scale Precipitation in Future Projections

The distinct vertical distributions of clouds can lead to varying climate responses to greenhouse gas emissions, contributing significantly to uncertainty in climate projec-

tions due to differences among models. This uncertainty remains one of the major challenges in accurately predicting future climate scenarios [54]. The vertical distribution of clouds [55,56] and moisture [57] is strongly linked to convective and large-scale precipitation components. These precipitation components are closely tied to different climate feedback mechanisms [58,59]. Furthermore, several studies have shown that correctly representing convective and large-scale rainfall [50,60] is crucial for better monsoon simulations, which may further improve representations of the Indian Summer Monsoon [37]. In view of this, an evaluation of convective and large-scale precipitation for observational, historical simulations is presented along with near-, mid-, and far-future terms spatially for the South Asian region (Figure 5).

Figure 5(a1,b1,c1) illustrates that under future greenhouse gas warming scenarios, convective precipitation increases gradually. The observational dataset provides a reference for analyzing rainfall patterns across the Western Ghats, Arabian Sea, Indian Ocean, northeastern India, and surrounding regions. Historical simulations replicate past convective rainfall patterns, capturing distributions with mean values of 6.34 mm/day over the Arabian Sea (65° E–74° E; 5° N–20° N) and 6.13 mm/day over the Eastern region (Bay of Bengal: 82° E–95° E; 5° N–20° N). Along the Myanmar coast (90° E–100° E; 10° N–20° N), historical simulations report extreme convective rainfall at 9.38 mm/day, providing a benchmark for comparison. In the mid-term (2041–2060), mean convective rainfall increases to 6.552 mm/day over the Arabian Sea, rising further to 7.32 mm/day in the far-future (2081–2100). Similarly, over the Bay of Bengal, convective precipitation increases from 6.91 mm/day in the near-term (2021–2040) to 6.78 mm/day in the mid-term and 7.94 mm/day in the far-future, surpassing historical values. Extreme convective rainfall along the Myanmar coast also intensifies, with mean values increasing to 10.20 mm/day in the near-term, 9.16 mm/day in the mid-term, and 11.44 mm/day in the far-future compared to 9.38 mm/day in historical simulations. These projections indicate amplified convective rainfall, particularly under global warming scenarios, with significant regional variations.

Total rainfall is the result of both convective and stratiform precipitation. Spatial features of large-scale precipitation during JJAS over the South Asian region under future scenarios are shown in Figure 5(a2,b2,c2). The observational dataset provides the baseline for assessing rainfall patterns across the Equatorial Indian Ocean, Tibetan Plateau, and Western Ghats. Historical simulations replicate observed rainfall distributions, offering a benchmark for detecting changes in large-scale precipitation under future scenarios. In the near-term (2021–2040), rainfall increases significantly along the Equatorial Indian Ocean (~2 mm/day) compared to historical simulations. The mid-term (2041–2060) and far-future (2081–2100) projections show enhanced large-scale rainfall along the Tibetan Plateau and Western Ghats, highlighting intensified regional precipitation under warming scenarios. Previous studies have found that significant cloud fractions at higher altitudes are due to the presence of anvil clouds, which produce stratiform rain [61]. This aligns with the present study, which also shows an increase in large-scale rainfall at higher altitudes.

The observational dataset provides the baseline for evaluating JJAS rainfall patterns over the Arabian Sea and Bay of Bengal. Historical simulations indicate mean stratiform rainfall values of 0.93 mm/day over the Arabian Sea and 1.05 mm/day over the Bay of Bengal. Future projections under SSP5-8.5 show a progressive increase in rainfall across both regions. In the Arabian Sea, mean JJAS rainfall rises to 1.05 mm/day in the near-term, 1.43 mm/day in the mid-term, and 1.92 mm/day in the far future. Similarly, over the Bay of Bengal, rainfall increases to 1.32 mm/day (near-term), 1.401 mm/day (mid-term), and 1.55 mm/day (far-future), highlighting amplified stratiform rainfall in warming scenarios. In this context, a study by [62] mentioned an increase in the precipitation over the Indian region using CMIP6 models in the far-future projection. Similarly, an increase

in the convective precipitation along the Asian region is demonstrated by [63] in the future scenarios.

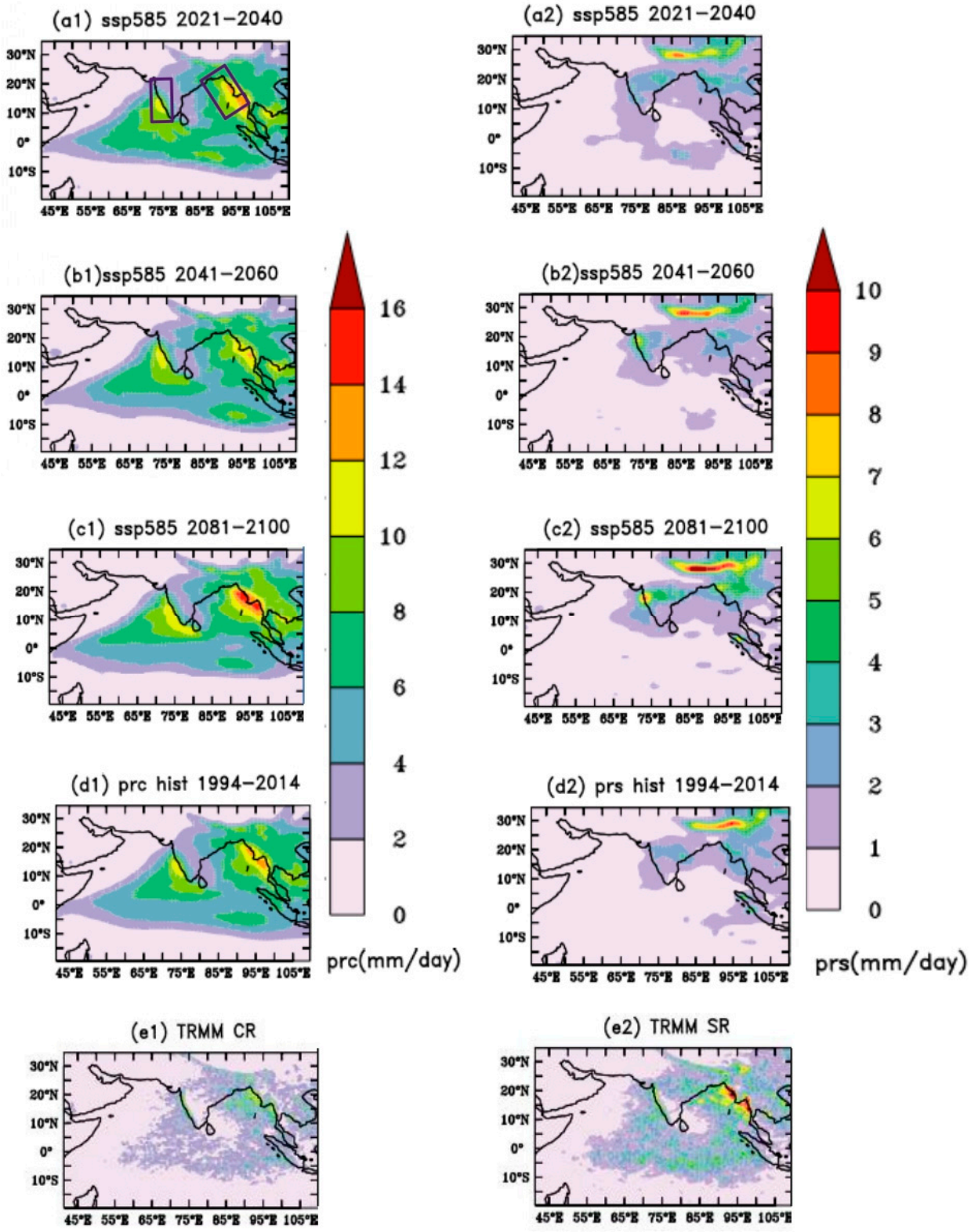


Figure 5. Convective precipitation for JJAS in near (2021–2040), mid (2041–2060) and far (2081–2100) SSP5-8.5 scenario (**a1**,**b1**,**c1**) along with historical (**d1**) and observational datasets (TRMM) (**e1**) along the 40° E-10° E to 20° S-40° N region. Large-scale precipitation in near (2021–2040), mid (2041–2060) and far (2081–2100) SSP5-8.5 scenario (**a2**,**b2**,**c2**) along with historical (**d2**) and observational dataset (TRMM) (**e2**) along South Asian region.

3.3. Cloud Simulations in Future Projections (High, Mid, and Low)

Different cloud types govern the Indian Summer Monsoon, such as stratus, stratocumulus, and deep convective clouds [64]. Clouds are classified as high, mid, or low based on cloud top pressures [51]. Figure 6 examines how different cloud levels are represented under greenhouse gas scenarios using the available multi-model ensemble (MME). Observations (CALIPSO-GOCCP) indicate that the Indian monsoon region is dominated by high-level clouds. Although the multi-model ensemble in historical simulations replicates high cloud cover, it tends to underestimate as compared to observations.

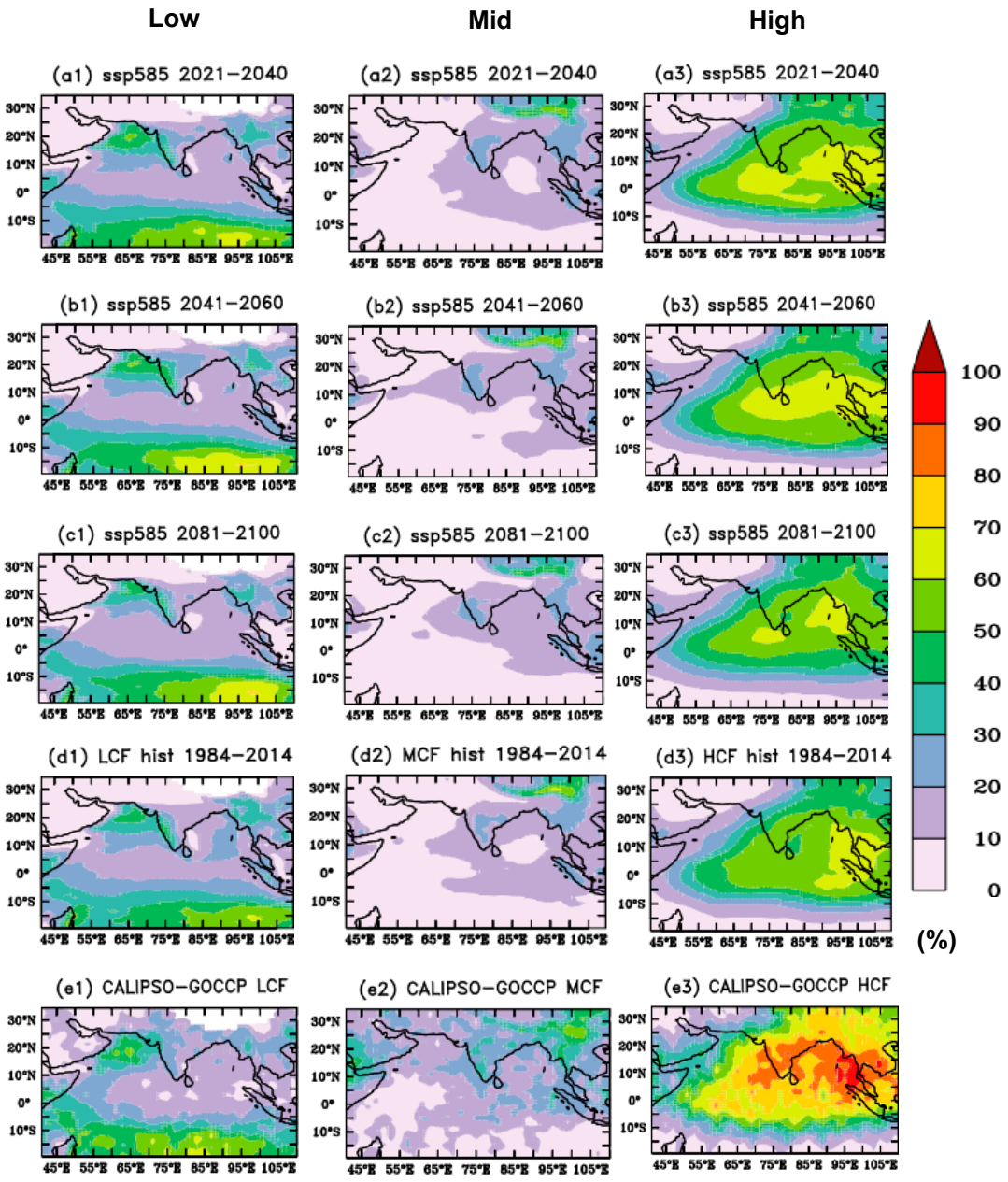


Figure 6. Spatial representation of Low (**left panel**), Mid (**center panel**), and High (**right panel**) cloud cover for JJAS in near-, mid-, and far-future projections compared to historical and observational dataset (CALIPSO-GOCCP).

High cloud cover predominantly blankets oceanic areas in the near- (2021–2040) and mid-future (2041–2060) periods, but it is projected to decline in the far-future (2081–2100) compared to historical simulations. Likewise, mid- and low-level cloud cover is seen to

be more significant over the Indian region during the near- (2021–2040) and mid-future (2041–2060) terms compared to the far-future and historical simulations.

Generally, changes in the different types of cloud cover are noticeable under climate change, with each cloud type responding differently to anthropogenic forcing. Correlation analysis suggests that while the spatial pattern of cloud types may remain largely unchanged due to climate change, the fractional coverage of each cloud type is significantly affected (e.g., [40]).

3.4. Association of Outgoing Longwave Radiation (OLR) with Total Cloud Fraction

Convection has strong and intricate interactions with radiative heating due to the diversity of cloud formations and convective behaviors [65]. Therefore, it is important to study the impact of OLR on clouds and its strength in future scenarios. The climatology of OLR, a proxy for convection [66,67], over the South Asian region is shown in Figure 7 using NOAA data. It is further compared with the CMIP6 multi-model ensemble for past and future scenarios. The observational dataset shows a mean outgoing longwave radiation (OLR) of 219.4 W/m^2 across the Indian landmass (Central India) and Arabian Sea (230.5 W/m^2). The historical simulations show an upsurge in the OLR values along the Central India region as compared to the observational dataset. Future projections, however, (Figure 7) indicate a decrease in OLR values along the oceanic region (Arabian Sea and Bay of Bengal) as compared to the Indian land mass indicating an intensification under warming scenarios. In the tropics, OLR variability is largely associated with high-altitude clouds and deep convection, exhibiting correspondingly complex behavior [65]. This study aligns with these findings, as low OLR is seen in all future terms, particularly over the Arabian Sea and Bay of Bengal, indicating deep convection activity (high clouds).

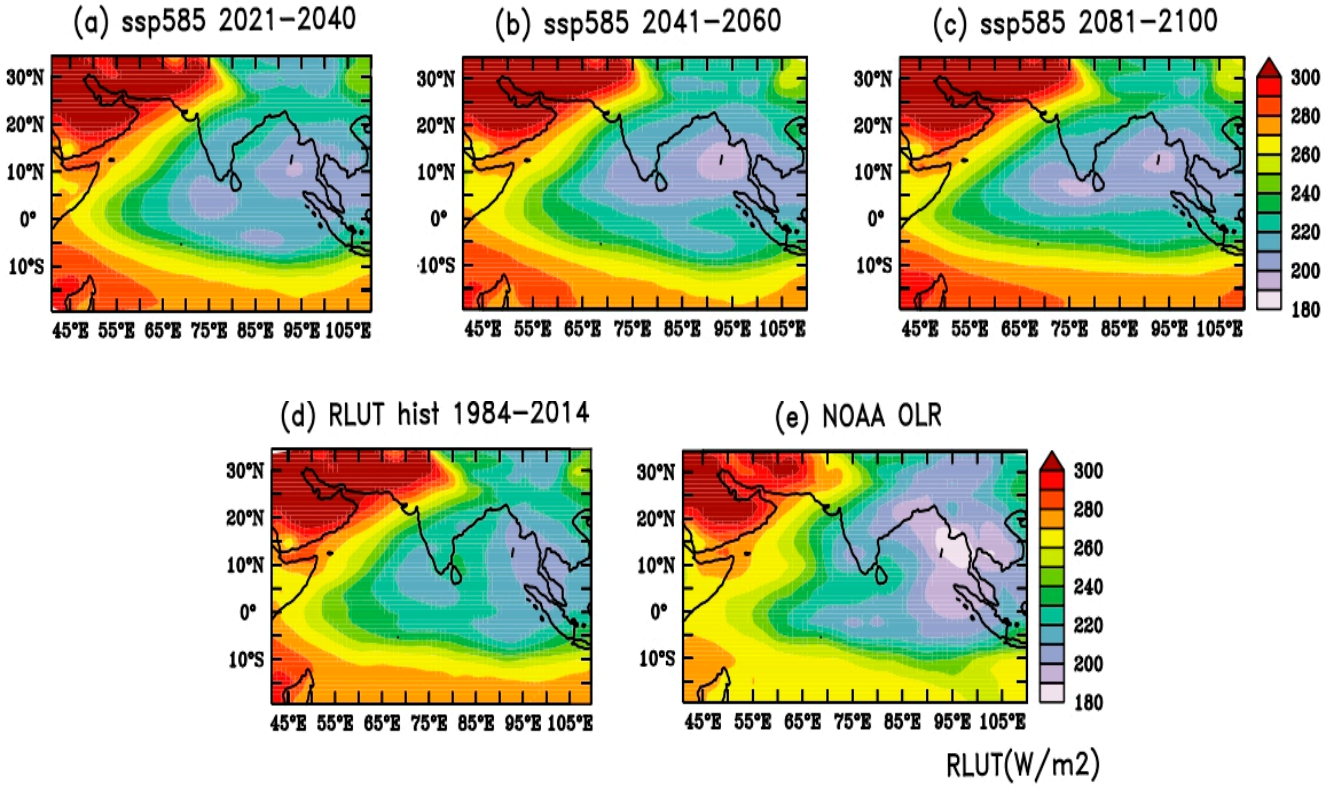


Figure 7. Spatial representation of outgoing longwave radiation for JJAS (OLR) along the South Asian region in MME's of future scenario's (near, mid, and far), historical and observational datasets (NOAA).

The pattern correlation between the multi-model ensemble for the historical simulations, near- (2021–2040) and mid-term (2041–2060) show similar values (PCC ~0.819, 0.808,

0.807) compared to the observed OLR pattern (Table 3) over the Indian region (65° E–95° E, 5° N–40° N).

Table 3. Pattern correlation between the model ensemble for Total Cloud Fraction (TCF), Total precipitation, Outgoing Longwave Radiation (OLR) in SSP5-8.5 scenario and observation over the Indian region (65° E–95° E, 5° N–40° N).

P.C.	TCF	Total Precip.	OLR
Ensemble 2021–2040	0.829	0.7409	0.8082
Ensemble 2041–2060	0.846	0.6952	0.8077
Ensemble 2081–2100	0.8097	0.6739	0.7755
Ensemble historical	0.8039	0.7245	0.8193

However, the pattern correlation for the far-future scenario (PCC ~0.77) underestimates the historical and other future scenarios, likely due to discrepancies in model cloud and radiative properties in far-future projections. A low correlation in OLR usually indicates a discrepancy in cloud cover, thickness, or altitude at low and mid-levels. Similarly, when compared with observational datasets and historical simulations (PCC ~0.803), total cloud fraction (TCF) shows consistency in the near-, mid-, and far-future terms' pattern correlation (PCC ~0.829, 0.846, 0.809).

In order to measure the average magnitude of errors between predicted and observed values in a model, the Root Mean Square Error is calculated (Table 4). RMSE is widely used to evaluate model accuracy. Hence, it is evaluated for precipitation, total cloud fraction, and outgoing longwave radiation. Table 1 indicates that the E3SM model shows the least error for precipitation, the MIROC model for OLR, and again the E3SM model for TCF. However, no single model demonstrates consistent accuracy across all atmospheric variables in terms of RMSE.

Table 4. Root Mean Square Error in CMIP6 models for Precipitation, Total Cloud Fraction, and Outgoing Longwave Radiation.

	40° E–110° E; 20° S–35° N		
Models	**Precipitation (1984–2014)**	**Outgoing Longwave Radiation (1984–2014)**	**Total Cloud Fraction (2006–2014)**
E3SM-1-0	6.586	52.46	82.11
IPSL-CM6A-LR	6.954	46.21	120.2
MIROC6	9.001	44.5	91.79
MRI-ESM2-0	8.327	58.63	106

A quantitative analysis of high cloud fraction and convective precipitation is performed by assessing the climatological JJAS mean value for the far-future term (2081–2100). Figure 8 presents a bar plot for different regions across the South Asian region. The observational dataset provides a baseline for high cloud cover and convective precipitation across the Bay of Bengal, Arabian Sea, Indian region, and Tibetan Plateau. Historical simulations closely replicate these patterns, serving as a benchmark. In the near- (2021–2040) and mid-term (2041–2060), moderate increases in high cloud cover and convective precipitation are observed across these regions. The far-future term (2081–2100) shows significant intensification of both variables compared to historical simulations, particularly under warming scenarios (Table 5). An increase in the high cloud fraction can be observed from SSP5-8.5 along the Arabian Sea (50.16), Bay of Bengal (61.64) as compared to historical simulation

(Table 5a). Similarly, for convective precipitation an increase can be visualized along the Indian region (4.69), Arabian Sea (7.32) and Bay of Bengal (7.94) for the high emission scenario (Table 5b).

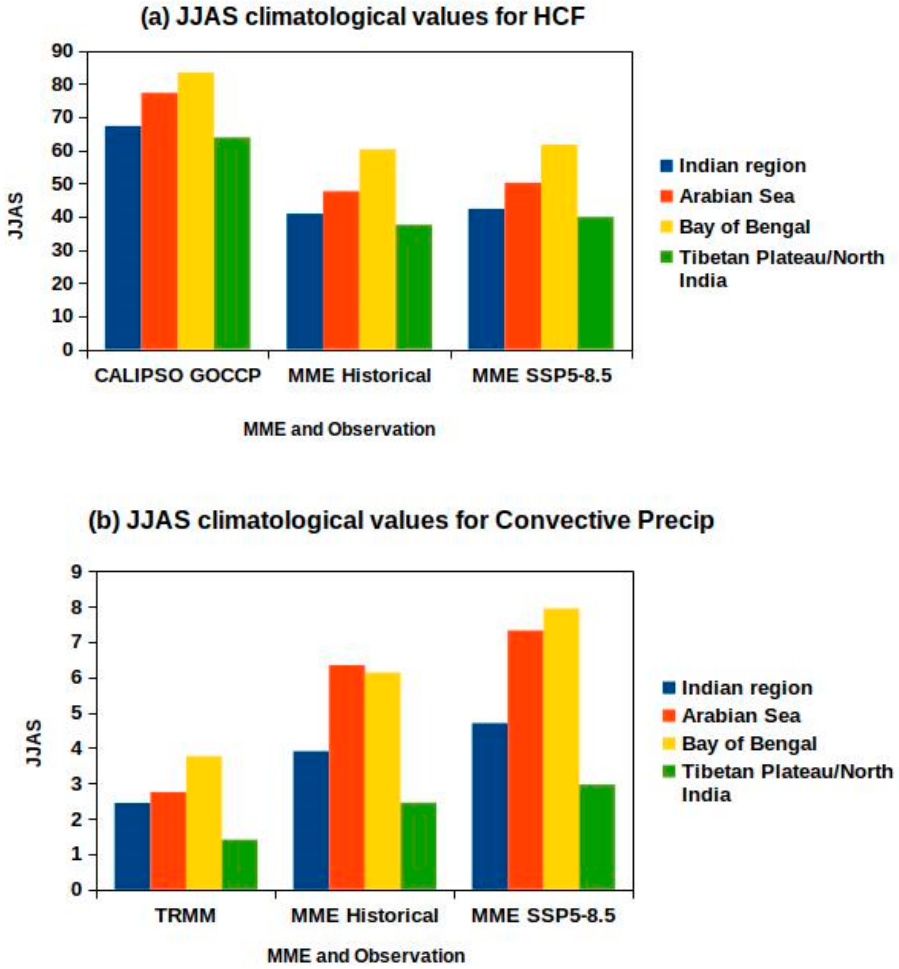


Figure 8. Bar-plot representing the climatological mean value for JJAS in High cloud cover (**a**) and Convective precipitation (**b**) along the various South Asian regions [Indian region (averaged over 65° E–95° E; 5° N–40° N) Arabian Sea (averaged over 65° E–74° E; 5° N–20° N), Bay of Bengal (averaged over 82° E–95° E; 5° N–20° N), Tibetan Plateau (averaged over 75° E–102° E; 25° N–37° N)].

Table 5. (**a**) Mean JJAS value for High Cloud Fraction under SSP5-8.5 far-future (2081–2100) projection for different regions (area mentioned in Figure 8), (**b**) Mean JJAS value for Convective Precipitation under SSP5-8.5 far-future (2081–2100) projection for different regions (area mentioned in Figure 8).

(**a**)				
High Cloud Fraction (%)	**Indian Region**	**Arabian Sea**	**Bay of Bengal**	**Tibetan Plateau**
CALIPSO GOCCP	67.24	77.21	83.36	63.79
MME Historical	40.82	47.59	60.22	37.5
MME SSP5-8.5	42.29	50.16	61.64	39.87
(**b**)				
Convective Precip. (mm/day)	**Indian Region**	**Arabian Sea**	**Bay of Bengal**	**Tibetan Plateau**
TRMM	2.44	2.751	3.765	1.404
MME Historical	3.901	6.34	6.131	2.449
MME SSP5-8.5	4.698	7.32	7.943	2.959

Majorly, the convective precipitation is heavily impacted by the volume of moisture transport from the oceans, which is observable from the bar-plot (Figure 8). Thus, an increase in precipitation concentration and high cloud content in future projections is evident from the above plot.

4. Conclusions

This study investigates the impact of future global warming on precipitating clouds and radiative dynamics using the CMIP6 multi-model ensemble. Also, this study highlights the relationship between precipitation and cloud types, categorizing them based on pressure levels (low, mid, and high) and their vertical distribution (convective and stratiform). Additionally, it examines the interconnection between outgoing longwave radiation and cloud properties [68,69]. It is true that model simulated clouds have limitations. However, the analysis provides valuable insights into how CMIP6 models represent vital atmospheric components in both past and future scenarios. The Shared Socio-Economic Pathway (SSP5-8.5) used is dominated by greenhouse gas forcing, which presents high challenges for mitigation. The multi-model ensemble is derived from the available atmosphere–ocean general circulation models (AOGCMs) to represent the regional characteristics of precipitation, cloud dynamics, and OLR. The major findings are as follows along the South Asian region:

1. The AOGCMs (Atmosphere–Ocean General Circulation Models) multi-model ensemble, despite their relatively coarse resolution, demonstrates reasonable skill in depicting the climatological mean JJAS cycle of rainfall along the Indian region. In the near-term (2021–2040), the region experiencing peak rainfall (~2 mm/day) shifts northward to approximately 28° N compared to current observations. In the mid-term (2041–2060), this rainfall persists into September, unlike historical patterns where it decreases north of 5° N. An increase in precipitation (~1.5 mm/day) is observed in the far-future term (2081–2100), particularly in October.
2. The northward progression of the Indian Summer Monsoon is reasonably well-captured by the multi-model ensembles across all timeframes: near-term (2021–2040), mid-term (2041–2060), and far-future (2081–2100), aligning closely with observational and historical simulations (1984–2014). The far-future projection (2081–2100) indicates an intensification of the rainfall pattern extending beyond the monsoon season (June to September), likely due to climate changes driven by greenhouse gas emissions.
3. Total cloud fraction and convection are crucial for the seasonal mean Indian Summer Monsoon Rainfall (ISMR). The seasonal mean total cloud fraction in the multi-model ensemble shows an increase in future projections (near: 55.49%, mid: 55.48%, far: 54.45%) compared to historical simulations (53.87%), indicating an amplification of cloud cover in the coming periods.
4. The vertical distribution of clouds is strongly linked with convective and stratiform precipitation. Therefore, there is an observed increase in convective zones (Western Ghats, Bay of Bengal, Indian Ocean). Convective rainfall increases in the near- (3.261 mm/day), mid- (3.158 mm/day), and far-future (3.302 mm/day) periods compared to historical simulations (3 mm/day). Similarly, stratiform precipitation increases in large-scale areas majorly along the Western Ghats and Tibetan Plateau in the near- (0.904 mm/day), mid- (0.852 mm/day), and far-future (0.962 mm/day) periods as compared to historical simulations (0.822 mm/day) during ISMR.
5. Since OLR is considered a proxy for convection, spatial coverage shows a decrease in OLR along the Arabian Sea, Bay of Bengal, and other regions coinciding with the presence of high cloud cover. The pattern correlation between the model ensemble and the observational dataset for total cloud fraction in the near-, mid-, and far-future

terms (PCC ~0.829, 0.846, 0.809) increases compared to historical simulations (PCC ~0.803). However, the pattern correlation for OLR in far-future projections (2081–2100) (PCC ~0.77) is relatively low compared to historical simulations (PCC ~0.819), likely due to model discrepancies in representing cloud levels.

Clouds remain a primary source of uncertainty in representing precipitation and radiative balances. While CMIP6 represents a step forward in simulating clouds, significant uncertainties remain, particularly concerning cloud feedback and their role in amplifying or dampening climate change. Therefore, as the global temperature rises, and where the future scenario (SSP5-8.5) depicts an increase in severe climatic conditions, it is crucial for models to overcome these uncertainties for better climate predictions.

Author Contributions: Conceptualization, R.L.B. and P.K.; methodology, R.L.B. and P.K.; software, P.K.; validation, R.L.B., P.K. and H.S.C.; formal analysis, R.L.B.; investigation, V.K. and H.S.C.; resources, R.L.B., HC and V.K.; data curation, P.K.; writing—original draft preparation, R.L.B. and P.K.; writing—review and editing, R.L.B., P.K., V.K. and H.S.C.; visualization, P.K.; supervision, R.L.B., H.S.C. and V.K.; project administration, R.L.B.; funding acquisition, R.L.B. and V.K. All authors have read and agreed to the published version of the manuscript.

Funding: This research received no external funding.

Data Availability Statement: All data used in this study are freely available in the public domain. The Coupled Model Inter-comparison Projects (CMIP6) data are collected from World Climate Research Program and available at the Earth System Grid Federation (ESGF, https://esgf-node.llnl.gov/) (accessed on 1 June 2024). Monthly data of total cloud fraction (TCF) are obtained from the GCM-Oriented CALIPSO Cloud Product (GOCCP, [45]) for 2006–2017 (12 years), available at: https://climatedataguide.ucar.edu/ (accessed on 26 September 2022). The OLR data are used from https://psl.noaa.gov/data/gridded/data.olrcdr.interp.html [49], (accessed on 17 December 2023). The GPCP rainfall data are available at (http://www.esrl.noaa.gov/psd/data/gridded/data.gpcp.html) [48] (accessed on 18 February 2022).

Acknowledgments: We thank the Department of Physics and Department of Atmospheric and Space Sciences, SPPU for providing support in completing this work. PK gratefully acknowledges support from FERCC for providing fellowship to carry out the work. We acknowledge the climate modeling groups for providing their model output via World Climate Research Program, the Earth System Grid Federation (ESGF, https://esgf-node.llnl.gov/), the CALIPSO-GOCCP (https://climatedataguide.ucar.edu/) [13], OLR data are used from https://psl.noaa.gov/data/gridded/data.interp_OLR.html [49] (accessed on 17 December 2023) and the GPCP (http://www.esrl.noaa.gov/psd/data/gridded/data.gpcp.html) [48] (accessed on 18 February 2022). We also thank the publicly available softwares viz., Ferret-NOAA, Climate Data Operators (CDO). This work is part of the PhD Thesis of the first author (PK).

Conflicts of Interest: The authors declare that they have no conflict of interest.

References

1. Parthasarathy, B.; Munot, A.A.; Kothawale, D.R. Regression model for estimation of indian foodgrain production from summer monsoon rainfall. *Agric. For. Meteorol.* **1988**, *42*, 167–182. [CrossRef]
2. Auffhammer, M.; Ramanathan, V.; Vincent, J.R. Integrated model shows that atmospheric brown clouds and greenhouse gases have reduced rice harvests in India. *Proc. Natl. Acad. Sci. USA* **2006**, *103*, 19668–19672. [CrossRef] [PubMed]
3. Kripalani, R.H.; Kulkarni, A.; Sabade, S.S.; Khandekar, M.L. Indian monsoon variability in a global warming scenario. *Nat. Hazards* **2003**, *29*, 189–206. [CrossRef]
4. Webster, P.J. Response of the tropical atmosphere to local, steady forcing. *Mon. Weather. Rev.* **1972**, *100*, 518–541. [CrossRef]
5. Kumar, K.R.; Pant, G.B.; Parthasarathy, B.; Sontakke, N.A. Spatial and subseasonal patterns of the long-term trends of Indian summer monsoon rainfall. *Int. J. Clim.* **1992**, *12*, 257–268. [CrossRef]
6. Guhathakurta, P.; Rajeevan, M. Trends in the rainfall pattern over India. *Int. J. Climatol. A J. R. Meteorol. Soc.* **2008**, *28*, 1453–1469. [CrossRef]

7. Yin, X.; Gruber, A.; Arkin, P. Comparison of the GPCP and CMAP merged gauge–satellite monthly precipitation products for the period 1979–2001. *J. Hydrometeorol.* **2004**, *5*, 1207–1222. [CrossRef]
8. Zhang, B.; Song, S.; Wang, H.; Guo, T.; Ding, Y. Evaluation of the performance of CMIP6 models in simulating extreme precipitation and its projected changes in global climate regions. *Nat. Hazards* **2024**, *121*, 1737–1763. [CrossRef]
9. Kitoh, A.; Yukimoto, S.; Noda, A.; Motoi, T. Simulated changes in the Asian summer monsoon at times of increased atmospheric CO_2. *J. Meteorol. Soc. Jpn. Ser. II* **1997**, *75*, 1019–1031. [CrossRef]
10. Hu, Z.; Latif, M.; Roeckner, E.; Bengtsson, L. Intensified Asian summer monsoon and its variability in a coupled model forced by increasing greenhouse gas concentrations. *Geophys. Res. Lett.* **2000**, *27*, 2681–2684. [CrossRef]
11. Lal, M.; Nozawa, T.; Emori, S.; Harasawa, H.; Takahashi, K.; Kimoto, M.; Abe-Ouchi, A.; Nakajima, T.; Takemura, T.U.; Numaguti, A. Future climate change: Implications for Indian summer monsoon and its variability. *Curr. Sci.* **2001**, *81*, 1196–1207.
12. May, W. Simulated changes of the Indian summer monsoon under enhanced greenhouse gas conditions in a global time-slice experiment. *Geophys. Res. Lett.* **2002**, *29*, 22-1–22-4. [CrossRef]
13. Kripalani, R.H.; Oh, J.H.; Kulkarni, A.; Sabade, S.S.; Chaudhari, H.S. South Asian summer monsoon precipitation variability: Coupled climate model simulations and projections under IPCC AR4. *Theor. Appl. Clim.* **2007**, *90*, 133–159. [CrossRef]
14. Khardekar, P.; Dutta, U.; Chaudhari, H.S.; Bhawar, R.L.; Hazra, A.; Pokhrel, S. Increase in Indian summer monsoon precipitation as a response to doubled atmospheric CO_2: CMIP6 simulations and projections. *Theor. Appl. Clim.* **2023**, *154*, 1233–1252. [CrossRef]
15. Hsu, P.; Li, T.; Luo, J.; Murakami, H.; Kitoh, A.; Zhao, M. Increase of global monsoon area and precipitation under global warming: A robust signal? *Geophys. Res. Lett.* **2012**, *39*. [CrossRef]
16. Christensen, J.H.; Kanikicharla, K.K.; Aldrian, E.; An, S.I.; Cavalcanti, I.F.A.; de Castro, M.; Dong, W.; Goswami, P.; Hall, A.; Kanyanga, J.K.; et al. Climate phenomena and their relevance for future regional climate change. In *Climate Change 2013 the Physical Science Basis: Working Group I Contribution to the Fifth Assessment Report of the Intergovernmental Panel on Climate Change*; Cambridge University Press: Cambridge, UK, 2013; pp. 1217–1308.
17. Chaturvedi, R.K.; Joshi, J.; Jayaraman, M.; Bala, G.; Ravindranath, N.H. Multi-model climate change projections for India under representative concentration pathways. *Curr. Sci.* **2012**, *103*, 791–802.
18. Menon, A.; Levermann, A.; Schewe, J.; Lehmann, J.; Frieler, K. Consistent increase in Indian monsoon rainfall and its variability across CMIP-5 models. *Earth Syst. Dyn.* **2013**, *4*, 287–300. [CrossRef]
19. Kamruzzaman, M.; Shahid, S.; Islam, A.T.; Hwang, S.; Cho, J.; Zaman, A.U.; Ahmed, M.; Rahman, M.; Hossain, B. Comparison of CMIP6 and CMIP5 model performance in simulating historical precipitation and temperature in Bangladesh: A preliminary study. *Theor. Appl. Clim.* **2021**, *145*, 1385–1406. [CrossRef]
20. Li, Z.; Liu, T.; Huang, Y.; Peng, J.; Ling, Y. Evaluation of the CMIP6 precipitation simulations over global land. *Earth's Futur.* **2022**, *10*, e2021EF002500. [CrossRef]
21. Puviarasan, N.; Sharma, A.; Ranalkar, M.; Giri, R. Onset, advance and withdrawal of southwest monsoon over Indian subcontinent: A study from precipitable water measurement using ground based GPS receivers. *J. Atmos. Solar-Terr. Phys.* **2015**, *122*, 45–57. [CrossRef]
22. Khadgarai, S.; Kumar, V.; Pradhan, P.K. The Connection between Extreme Precipitation Variability over Monsoon Asia and Large-Scale Circulation Patterns. *Atmosphere* **2021**, *12*, 1492. [CrossRef]
23. Sperber, K.R.; Palmer, T.N. Interannual tropical rainfall variability in general circulation model simulations associated with the Atmospheric Model Intercomparison Project. *J. Clim.* **1996**, *9*, 2727–2750. [CrossRef]
24. Goswami, B.N. Interannual variations of Indian summer monsoon in a GCM: External conditions versus internal feedbacks. *J. Clim.* **1998**, *11*, 501–522. [CrossRef]
25. Kucharski, F.; Bracco, A.; Yoo, J.H.; Tompkins, A.M.; Feudale, L.; Ruti, P.; Dell'Aquila, A. A Gill–Matsuno-type mechanism explains the tropical Atlantic influence on African and Indian monsoon rainfall. *Q. J. R. Meteorol. Soc. A J. Atmos. Sci. Appl. Meteorol. Phys. Oceanogr.* **2009**, *135*, 569–579. [CrossRef]
26. Ramanathan, V.; Barkstrom, B.R.; Harrison, E.F. Climate and the Earth's radiation budget. *Phys. Today* **1989**, *42*, 22–32. [CrossRef]
27. Weare, B.C. Climatic variability of cloud radiative forcing. *Q. J. R. Meteorol. Soc.* **1997**, *123*, 1055–1073. [CrossRef]
28. Zelinka, M.D.; Myers, T.A.; McCoy, D.T.; Po-Chedley, S.; Caldwell, P.M.; Ceppi, P.; Klein, S.A.; Taylor, K.E. Causes of higher climate sensitivity in CMIP6 models. *Geophys. Res. Lett.* **2020**, *47*, e2019GL085782. [CrossRef]
29. Bony, S.; Stevens, B.; Frierson, D.M.W.; Jakob, C.; Kageyama, M.; Pincus, R.; Shepherd, T.G.; Sherwood, S.C.; Siebesma, A.P.; Sobel, A.H.; et al. Clouds, circulation and climate sensitivity. *Nat. Geosci.* **2015**, *8*, 261–268. [CrossRef]
30. Dutta, U.; Chaudhari, H.S.; Hazra, A.; Pokhrel, S.; Saha, S.K.; Veeranjaneyulu, C. Role of convective and microphysical processes on the simulation of monsoon intraseasonal oscillation. *Clim. Dyn.* **2020**, *55*, 2377–2403. [CrossRef]
31. Hazra, A.; Chaudhari, H.S.; Saha, S.K.; Pokhrel, S. Effect of cloud microphysics on Indian summer monsoon precipitating clouds: A coupled climate modeling study. *J. Geophys. Res. Atmos.* **2017**, *122*, 3786–3805. [CrossRef]
32. Eyring, V.; Bony, S.; Meehl, G.A.; Senior, C.A.; Stevens, B.; Stouffer, R.J.; Taylor, K.E. Overview of the Coupled Model Intercomparison Project Phase 6 (CMIP6) experimental design and organization. *Geosci. Model Dev.* **2016**, *9*, 1937–1958. [CrossRef]

33. Riahi, K.; Van Vuuren, D.P.; Kriegler, E.; Edmonds, J.; O'Neill, B.C.; Fujimori, S.; Bauer, N.; Calvin, K.; Dellink, R.; Fricko, O.; et al. The Shared Socioeconomic Pathways and their energy, land use, and greenhouse gas emissions implications: An overview. *Glob. Environ. Change* **2017**, *42*, 153–168. [CrossRef]
34. O'Neill, B.C.; Tebaldi, C.; van Vuuren, D.P.; Eyring, V.; Friedlingstein, P.; Hurtt, G.; Knutti, R.; Kriegler, E.; Lamarque, J.-F.; Lowe, J.; et al. The scenario model intercomparison project (ScenarioMIP) for CMIP6. *Geosci. Model Dev.* **2016**, *9*, 3461–3482. [CrossRef]
35. Bock, L.; Lauer, A.; Schlund, M.; Barreiro, M.; Bellouin, N.; Jones, C.; Meehl, G.A.; Predoi, V.; Roberts, M.J.; Eyring, V. Quantifying progress across different CMIP phases with the ESMValTool. *J. Geophys. Res. Atmos.* **2020**, *125*, e2019JD032321. [CrossRef]
36. Lauer, A.; Bock, L.; Hassler, B.; Schröder, M.; Stengel, M. Cloud climatologies from global climate models—A comparison of CMIP5 and CMIP6 models with satellite data. *J. Clim.* **2023**, *36*, 281–311. [CrossRef]
37. Chaudhari, H.S.; Hazra, A.; Pokhrel, S.; Saha, S.K.; Talluri, S.S. Simulation of extreme Indian summer monsoon years in Coupled Model Intercomparison Project Phase 5 models: Role of cloud processes. *Int. J. Clim.* **2018**, *39*, 901–920. [CrossRef]
38. Fischer, E.M.; Knutti, R. Observed heavy precipitation increase confirms theory and early models. *Nat. Clim. Change* **2016**, *6*, 986–991. [CrossRef]
39. Trenberth, K.E. Conceptual Framework for Changes of Extremes of the Hydrological Cycle with Climate Change. *Clim. Change* **1999**, *42*, 327–339. [CrossRef]
40. Luo, H.; Quaas, J.; Han, Y. Examining cloud vertical structure and radiative effects from satellite retrievals and evaluation of CMIP6 scenarios. *Atmos. Chem. Phys.* **2023**, *23*, 8169–8186. [CrossRef]
41. Golaz, J.; Caldwell, P.M.; Van Roekel, L.P.; Petersen, M.R.; Tang, Q.; Wolfe, J.D.; Abeshu, G.; Anantharaj, V.; Asay-Davis, X.S.; Bader, D.C.; et al. The DOE E3SM coupled model version 1: Overview and evaluation at standard resolution. *J. Adv. Model. Earth Syst.* **2019**, *11*, 2089–2129. [CrossRef]
42. Boucher, O.; Servonnat, J.; Albright, A.L.; Aumont, O.; Balkanski, Y.; Bastrikov, V.; Bekki, S.; Bonnet, R.; Bony, S.; Bopp, L.; et al. Presentation and evaluation of the IPSL-CM6A-LR climate model. *J. Adv. Model. Earth Syst.* **2020**, *12*, e2019MS002010. [CrossRef]
43. Tatebe, H.; Ogura, T.; Nitta, T.; Komuro, Y.; Ogochi, K.; Takemura, T.; Sudo, K.; Sekiguchi, M.; Abe, M.; Saito, F.; et al. Description and basic evaluation of simulated mean state, internal variability, and climate sensitivity in MIROC6. *Geosci. Model Dev.* **2019**, *12*, 2727–2765. [CrossRef]
44. Yukimoto, S.; Kawai, H.; Koshiro, T.; Oshima, N.; Yoshida, K.; Urakawa, S.; Tsujino, H.; Deushi, M.; Tanaka, T.; Hosaka, M.; et al. The Meteorological Research Institute Earth System Model version 2.0, MRI-ESM2. 0: Description and basic evaluation of the physical component. *J. Meteorol. Soc. Jpn. Ser. II* **2019**, *97*, 931–965. [CrossRef]
45. Chepfer, H.; Bony, S.; Winker, D.; Cesana, G.; Dufresne, J.L.; Minnis, P.; Stubenrauch, C.J.; Zeng, S. The GCM-oriented calipso cloud product (CALIPSO-GOCCP). *J. Geophys. Res. Atmos.* **2010**, *115*. [CrossRef]
46. Cesana, G.; Chepfer, H. How well do climate models simulate cloud vertical structure? A comparison between CALIPSO-GOCCP satellite observations and CMIP5 models. *Geophys. Res. Lett.* **2012**, *39*. [CrossRef]
47. Cesana, G.; Chepfer, H. Evaluation of the cloud thermodynamic phase in a climate model using CALIPSO-GOCCP. *J. Geophys. Res. Atmos.* **2013**, *118*, 7922–7937. [CrossRef]
48. Adler, R.F.; Huffman, G.J.; Chang, A.; Ferraro, R.; Xie, P.; Janowiak, J.; Rudolf, B.; Schneider, U.; Curtis, S.; Bolvin, D.; et al. The version 2 Global Precipitation Climatology Project (GPCP) monthly precipitation analysis (1979-present). *J. Hydrometeorol.* **2003**, *4*, 1147–1167. [CrossRef]
49. Liebmann, B.; Smith, C.A. Description of a complete (interpolated) outgoing longwave radiation dataset. *Bull. Am. Meteorol. Soc.* **1996**, *77*, 1275–1277.
50. Pokhrel, S.; Sikka, D.R. Variability of the TRMM-PR total and convective and stratiform rain fractions over the Indian region during the summer monsoon. *Clim. Dyn.* **2012**, *41*, 21–44. [CrossRef]
51. Chaudhari, H.S.; Pokhrel, S.; Kulkarni, A.; Hazra, A.; Saha, S.K. Clouds–SST relationship and interannual variability modes of Indian summer monsoon in the context of clouds and SSTs: Observational and modelling aspects. *Int. J. Clim.* **2016**, *36*, 4723–4740. [CrossRef]
52. Hong, Y.; Liu, G.; Li, J.-L.F. Assessing the radiative effects of global ice clouds based on CloudSat and CALIPSO measurements. *J. Clim.* **2016**, *29*, 7651–7674. [CrossRef]
53. Baker, M.B. Cloud microphysics and climate. *Science* **1997**, *276*, 1072–1078. [CrossRef]
54. Yang, J.; He, S.; Bao, Q. Convective/large-scale rainfall partitions of tropical heavy precipitation in CMIP6 atmospheric models. *Adv. Atmos. Sci.* **2021**, *38*, 1020–1027. [CrossRef]
55. Zhao, M. An investigation of the connections among convection, clouds, and climate sensitivity in a global climate model. *J. Clim.* **2014**, *27*, 1845–1862. [CrossRef]
56. Wang, Y.; Zhang, G.J. Global climate impacts of stochastic deep convection parameterization in the NCAR CAM 5. *J. Adv. Model. Earth Syst.* **2016**, *8*, 1641–1656. [CrossRef]
57. Bretherton, C.S.; Peters, M.E.; Back, L.E. Relationships between water vapor path and precipitation over the tropical oceans. *J. Clim.* **2004**, *17*, 1517–1528. [CrossRef]

58. Zelinka, M.D.; Klein, S.A.; Taylor, K.E.; Andrews, T.; Webb, M.J.; Gregory, J.M.; Forster, P.M. Contributions of different cloud types to feedbacks and rapid adjustments in CMIP5. *J. Clim.* **2013**, *26*, 5007–5027. [CrossRef]
59. Stephens, B.A.; Jackson, C.S.; Wagman, B.M. Effect of tropical nonconvective condensation on uncertainty in modeled projections of rainfall. *J. Clim.* **2019**, *32*, 6571–6588. [CrossRef]
60. Hazra, A.; Chaudhari, H.S.; Rao, S.A.; Goswami, B.N.; Dhakate, A.; Pokhrel, S.; Saha, S.K. Impact of revised cloud microphysical scheme in CFSv2 on the simulation of the Indian summer monsoon. *Int. J. Clim.* **2015**, *35*, 4738–4755. [CrossRef]
61. Sindhu, K.D.; Ratan, R. Cloud fraction biases in CALIPSO simulators of CMIP5 models over India. *Theor. Appl. Clim.* **2020**, *141*, 247–256. [CrossRef]
62. Krishnan, R.; Gnanaseelan, C.; Sanjay, J.; Swapna, P.; Dhara, C.; Sabin, T.P.; Jadhav, J.; Sandeep, N.; Choudhury, A.D.; Singh, M.; et al. Introduction to climate change over the Indian region. In *Assessment of Climate Change over the Indian Region: A Report of the Ministry of Earth Sciences (MoES), Government of India*; Springer: Berlin/Heidelberg, Germany, 2020; pp. 1–20.
63. Moon, S.; Ha, K.-J. Future changes in monsoon duration and precipitation using CMIP6. *npj Clim. Atmos. Sci.* **2020**, *3*, 45. [CrossRef]
64. Subrahmanyam, K.V.; Kumar, K.K. CloudSat observations of cloud-type distribution over the Indian summer monsoon region. *Ann. Geophys.* **2013**, *31*, 1155–1162. [CrossRef]
65. Zhang, K.; Randel, W.J.; Fu, R. Relationships between outgoing longwave radiation and diabatic heating in reanalyses. *Clim. Dyn.* **2016**, *49*, 2911–2929. [CrossRef]
66. Murakami, T. Temporal variations of satellite-observed outgoing longwave radiation over the winter monsoon region. Part I: Long-period (15–30 day) oscillations. *Mon. Weather Rev.* **1980**, *108*, 408–426. [CrossRef]
67. Prasad, K.D.; Verma, R.K. Large-scale features of satellite-derived outgoing long-wave radiation in relation to monsoon circulation over the indian region. *J. Climatol.* **1985**, *5*, 297–306. [CrossRef]
68. Lin, H.; Li, Z.; Li, J.; Zhang, F.; Min, M.; Menzel, W.P. Estimate of daytime single-layer cloud base height from advanced baseline imager measurements. *Remote Sens. Environ.* **2022**, *274*, 112970. [CrossRef]
69. Leena, P.P.; Mise, D.J.; Resmi, E.A.; Kumar, V.A.; Chakravarty, K.; Nirmin, K.S.; Kumar, P.P.; Patil, R.P.; Pandithurai, G. A Statistical Study on Cloud Base Height Behavior and Cloud Types During Southwest Monsoon over a High-Altitude Site in Western Ghats, India. *J. Indian Soc. Remote Sens.* **2024**, *52*, 203–217. [CrossRef]

Disclaimer/Publisher's Note: The statements, opinions and data contained in all publications are solely those of the individual author(s) and contributor(s) and not of MDPI and/or the editor(s). MDPI and/or the editor(s) disclaim responsibility for any injury to people or property resulting from any ideas, methods, instructions or products referred to in the content.